SCIENTIFIC REPORTS

OPEN

SUBJECT AREAS:
APPLIED PHYSICS
FLUID DYNAMICS
DESIGN, SYNTHESIS AND PROCESSING
MECHANICAL ENGINEERING

Received
27 June 2013

Accepted
31 October 2013

Published
19 November 2013

Correspondence and requests for materials should be addressed to Y.S.S. (ysong@dankook.ac.kr) or J.R.Y. (jaeryoun@snu.ac.kr)

Multiplex Particle Focusing via Hydrodynamic Force in Viscoelastic Fluids

Doo Jin Lee[1], Howard Brenner[2], Jae Ryoun Youn[1] & Young Seok Song[3]

[1]Research Institute of Advanced Materials (RIAM), Department of Materials Science and Engineering, Seoul National University, Daehak-Dong, Gwanak-Gu, Seoul 151-744, Korea, [2]Department of Chemical Engineering, Massachusetts Institute of Technology, Cambridge, Massachusetts 02139, USA, [3]Department of Fiber System Engineering, Dankook University, 126 Jukjeon-dong Suji-gu, Yongin-si, Gyeonggi-do 448-701, Korea.

We introduce a multiplex particle focusing phenomenon that arises from the hydrodynamic interaction between the viscoelastic force and the Dean drag force in a microfluidic device. In a confined microchannel, the first normal stress difference of viscoelastic fluids results in a lateral migration of suspended particles. Such a viscoelastic force was harnessed to focus different sized particles in the middle of a microchannel, and spiral channel geometry was also considered in order to take advantage of the counteracting force, Dean drag force that induces particle migration in the outward direction. For theoretical understanding, we performed a numerical analysis of viscoelastic fluids in the spiral microfluidic channel. From these results, a concept of the 'Dean-coupled Elasto-inertial Focusing band (DEF)' was proposed. This study provides in-depth physical insight into the multiplex focusing of particles that can open a new venue for microfluidic particle dynamics for a concrete high throughput platform at microscale.

Viscoelastic fluids, which can be encountered extensively in nature, demonstrate extraordinary physical phenomena due to their intrinsically viscous and elastic features. There are some intriguing examples related to the viscoelasticity: most biological cells produce extracellular polymeric substances (EPS), such as polysaccharides, nucleic acids, polypeptides, proteins, growth regulators, lipids, and a number of other compounds not yet fully characterized[1–4]. The protein secretion generates natural viscoelastic substances to protect cells from the harmful effect of toxic substances[3,5]. The most common fluid in our daily lives is saliva, the viscoelasticity of which forms a distinct beads-on-a-string (BOAS) structure[6]. Lastly, cells in a Newtonian medium experience viscoelastic deformation during the flow throughout vessels provoking viscoelasticity-induced force, which is used to isolate rare target cells from heterogeneous sample[7,8] and to separate normal erythrocytes from malaria-infected erythrocytes[9,10].

Very recently it has been revealed that the positive first normal stress difference (N_1) generated by the viscoelastic nature leads suspended particles or cells to migrate into certain positions in a confined microchannel[11–18]. Manipulating particle dynamics with help of the intrinsic properties of the medium is very desirable for easy, cost-effective, and continuous separation compared to conventional techniques such as filtration[19–21], electrophoresis[22], dielectrophoresis[23], and hydrodynamic chromatography[24–26]. Worth noting is that particles in the viscoelastic Poiseuille flow are migrated towards the center and four corners of the channel, i.e., the position with the minimum shear rate[13,18]. Moreover, the number of multiple equilibrium positions can be reduced to one equilibrium at the centerline by increasing the flow rate due to the synergetic effect of inertia and viscoelasticity[18]. The lateral migration of particles in the viscoelastic fluid is driven by the imbalance of the compressive nonlinear elastic forces, which are described in terms of the first and second normal stress differences, $N_1(\dot{\gamma}) = \sigma_{xx} - \sigma_{yy}$ and $N_2(\dot{\gamma}) = \sigma_{yy} - \sigma_{zz}$.

The Dean vortices, one of the secondary forces, can also contribute to particle migration. The fluid within the curved channel should satisfy the mass balance between inner-wall and outer-wall regions. This induces a pressure gradient in a radial direction, thereby generating two counter rotating vortices at the channel. This secondary flow is characterized by the Dean number, $De = Re_c \cdot \sqrt{D_h/2R}$, where Re_c is the channel Reynolds number, D_h is the hydrodynamic channel height, and R is the radius of curvature of the spiral channel. A recent study presents the balance between the inertial lift force, F_L, and the Dean drag force, $F_D \sim \rho U_m^2 a D_h^2 r^{-1}$, which

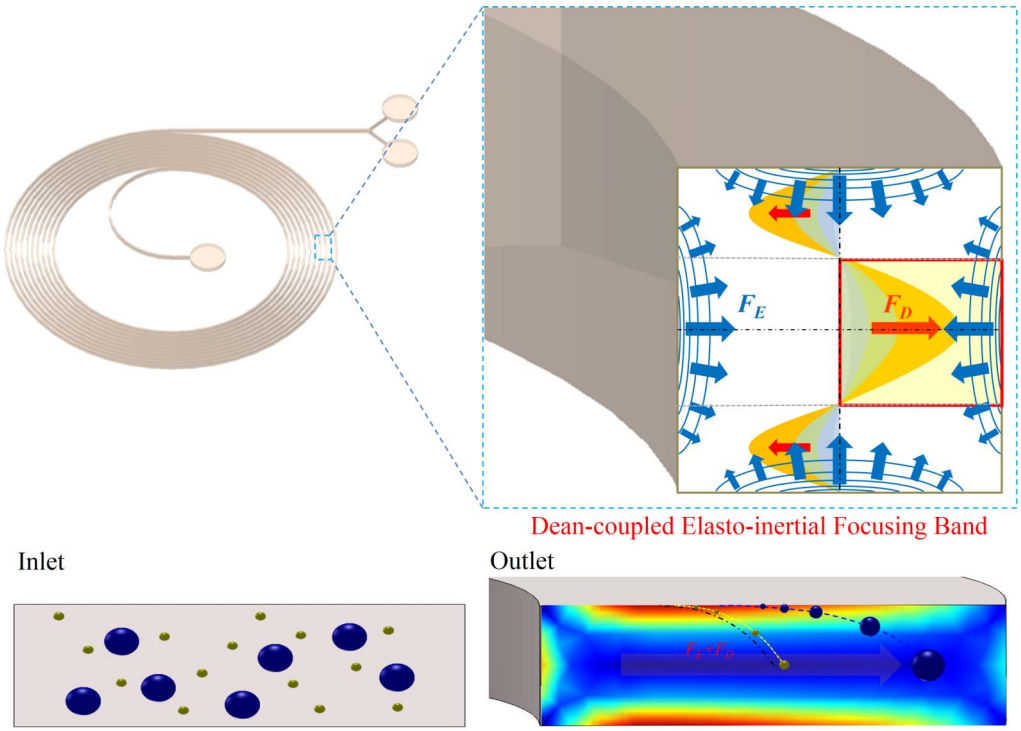

Figure 1 | Schematic representation of the Dean-coupled Elasto-inertial Focusing. Different sized particles are randomly injected into an inlet and displaced with differential lateral migration at an outlet. In a confined spiral channel, particles experience both elastic force and Dean drag force, the interaction of which determines equilibrium positions of the suspended particles.

determines the preferred location of particles in a curved channel[27,28]. When the density of a particle is larger than that of the surrounding medium, the particle subsides. In a similar way, larger particles can be collected in an outer wall with the aid of the characteristic velocity distribution on the cross-sectional plane normal to the main flow[29]. As the density of a particle is similar to that of the medium, the ratio of F_L/F_D is a determinant of the equilibrium positions. For instance, larger particles with higher F_L/F_D have a lateral migration towards the inner wall[30,31]. Thus, the scaling law between F_L and F_D acts as a dominant focusing factor: if the Dean flow is dominant (i.e., $F_D \gg F_L$), there is no focusing. Otherwise, focusing is favored due to the dominant inertial lift force. The scaling law, $F_L/F_D \sim (1/\delta)(a/D_h)^3 \mathrm{Re}_c^n$ $(n<0)$ containing parameters of Re_c and curvature ratio, δ, indicates that the ratio of particle size and channel dimension, a/D_h, plays an important role in determining the focusing behavior. For instance, small particles with large channel dimensions would not be focused. Preferential focusing of particles can only be achieved when a/D_h is larger than 0.07[30,32,33]. The aforementioned inertial microfluidics demonstrates that the defocusing of a particle occurs as F_D and Re_c increase. However, an equilibrium state is unstable since the superposition of inertial lift and Dean drag forces gives two modified stable equilibrium positions at which the balance is susceptible to be broken by the Dean vortices[28]. Consequently, no equilibrium position exists in that a particle size is much smaller than a microchannel or the balance of F_L/F_D breaks the criterion. In this respect geometry itself does not necessarily guarantee complete particle manipulation in a microchannel, while the elastic force driven by fluidic nature (i.e., the differential of N_1) can solely focus suspended particles in a line stably[7,15].

Here, we explore an extraordinary particle focusing in a microfluidic channel by probing two counteracting forces: one is an elastic force induced by the nature of a viscoelastic medium and the other is a Dean drag force resulting from the curved channel geometry. Also, we investigate the physical reasons for the multiplex particle focusing by numerical analysis and propose a new concept of the 'Dean-coupled Elasto-inertial Focusing (DEF)' band.

Results

Different sized particles are randomly injected into an inlet of a spiral channel using a viscoelastic medium (Fig. 1). In the confined spiral channel the particles undergo both of elastic force (F_E) and Dean drag force (F_D), which determines equilibrium positions of the suspended particles. As a result, The DEF band is created on the right side of the confined spiral channel (see the red-box in the cross-section of the channel). A narrow spiral channel with an aspect ratio (γ) is 0.25 shows different distribution of the first normal stress difference induced by the elastic nature of viscoelastic fluid, resulting in the focusing band and displacement of the different sized particles as shown in the outlet of the schematic representation. It should be noted that once particles are focused in the region of the DEF band, lateral migration is determined by the competition of F_D and F_E.

No particle focusing is observed at the outlet when each polystyrene (PS) particle with sizes of 1.5 μm, 5 μm, and 10 μm is used in a Newtonian medium (Fig. 2a ~ c and SI Fig. 1). However, particles were successfully focused when using a viscoelastic medium. Single-line particle focusing has been successfully achieved by using a viscoelastic medium, which is attributed to the combination of F_D and F_E. Also, the larger particles were found to move closer to the outer wall than the smaller particles. We also examined multiplex particle focusing using both small and large particles with diameters of 1.5 μm and 10 μm in a viscoelastic medium (Fig. 2g). It is expected that the particle to particle interaction would increase with increasing particle concentration, which induces the perturbation of flow and then prohibits the particle focusing. In this sense, a microfluidic system using hydrodynamics has not been regarded as a right tool for focusing size-dependent multiple cells or particles in a robust manner. It is shown that both the small and large particles flow randomly at the inlet and the randomness is still present at the

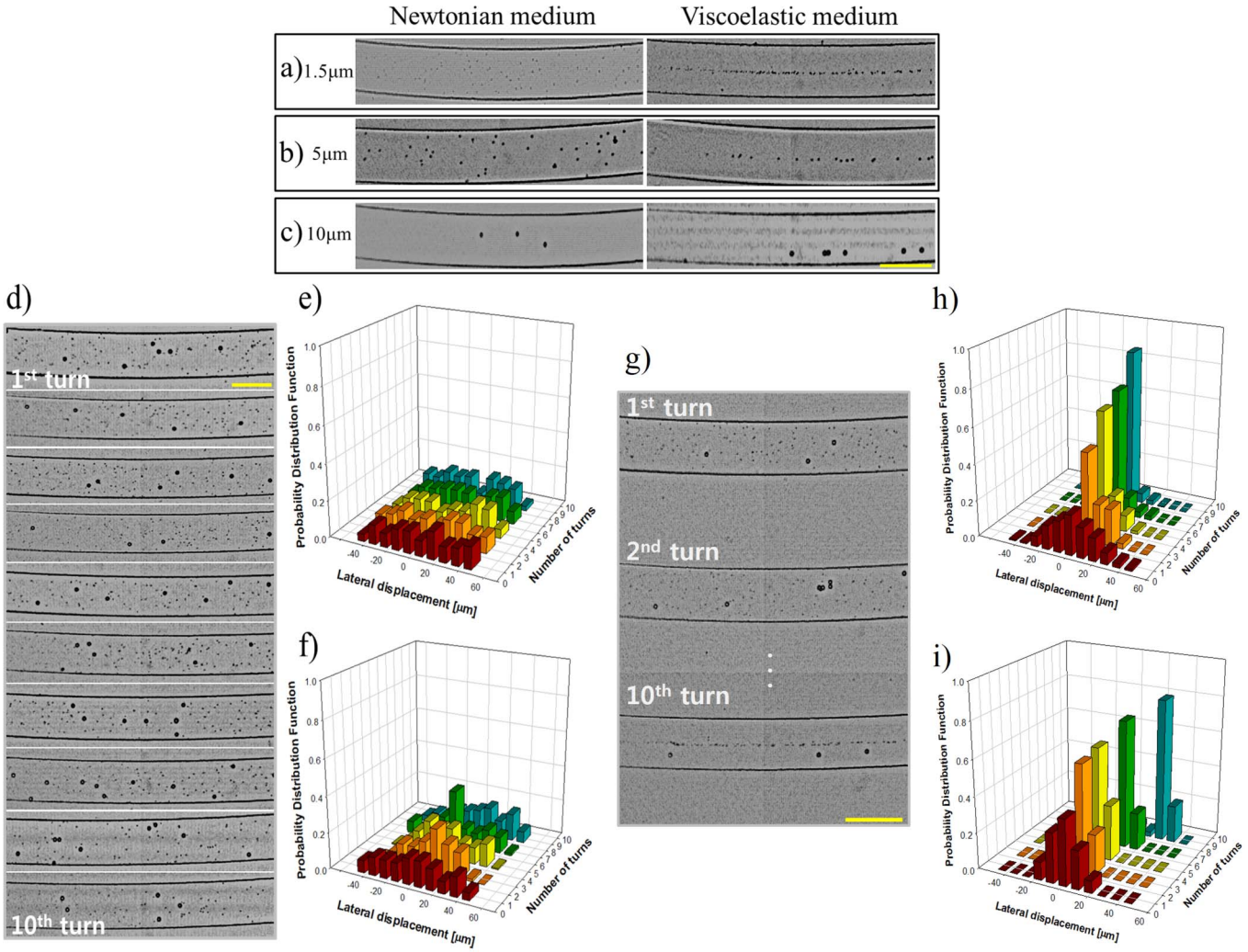

Figure 2 | Experimental results of particle dynamics in both the Newtonian and viscoelastic mediums. (a), (b) and (c) PS particles are not focused in the Newtonian medium but focused in the viscoelastic medium. (d) Dual PS particles with 1.5 and 10 μm are not focused in a Newtonian medium. (e) Probability distribution function of 1.5 μm PS particles with respect to the number of turns. (f) Probability distribution function of 10 μm PS particles with respect to the number of turns. (g) Dual PS particles with 1.5 and 10 μm are successfully focused with differential lateral migration in the viscoelastic medium. (h) Probability distribution function of 1.5 μm PS particles with respect to the number of turns, showing particle focusing at the center. (i) Probability distribution function of 10 μm PS particles with respect to the number of turns, showing particle focusing near the outer wall.

second turn of the spiral channel (Fig. 2g). After the particles experience the tenth turn, both the particles have different equilibrium positions, indicating that 1.5 μm PS particles are at the center line and 10 μm PS ones are close to the outer wall (Fig. 2g). The probability distribution function of both 1.5 and 10 μm PS with differential lateral migration elucidates the preferential particle focusing at the center for the small particle and near the outer wall for the large particle (Fig. 2h and 2i). However, both particles are not focused in a Newtonian medium even though the particles go through the tenth turn (Fig. 2d). The probability distribution function of both 1.5 and 10 μm PS with differential lateral migration shows that no particle focusing occurs regardless of the particle size (Fig. 2e and 2f). The results demonstrate that multiplex particle focusing is achievable using a hydrodynamic system through a viscoelastic medium without any external forces.

The different sized particles are entrained parallel, and bifurcate at the outlet: 1.5 μm PS particles towards the upper outlet and 10 μm PS ones towards the lower outlet (Fig. 3 and SI movie 4). The large particles with the diameter of 10 μm move closer to the outer wall of the microchannel due to the combination of the elastic and Dean drag forces. However, the small particles with the diameter of 1.5 μm are positioned at the center because the effect of the Dean drag force acting on the particles is comparably smaller than that of the elastic force. The lateral displacement of both particles was acquired and fitted by the Gaussian distribution function (see the inset in Fig. 3). There is no overlap between the lateral displacements of 1.5 μm and 10 μm PS particles, which guarantees high separating efficiency at the outlet.

It turns out that the high magnitude of N_1 appears near the inner wall in the cross-section of a straight channel (Fig. 4a and 4c). N_1 is not found in a Newtonian medium (meaning $Wi = 0$) since there is no elastic nature in the Newtonian fluid, thus being subject to only the Dean drag force and inertial lift force. The minimum values are found at four corners and the center as Wi becomes large, which leads particles to the center and the phenomenon is called as the 'elasto-inertial effect'[18]. The value of $N1/|N_1^{\max}|$ shows symmetry along the lateral position of the channel and increases with increasing Wi (Fig. 4c). In addition, the curvature of the spiral channel creates Dean vortices causing the lateral migration of the flow in the channel. Therefore, larger particles undergo more lateral migration on account of the increased De_p than smaller particles (Fig. 4b and SI movie 2). De_p corresponds to the particle dean number with 1.5, 5,

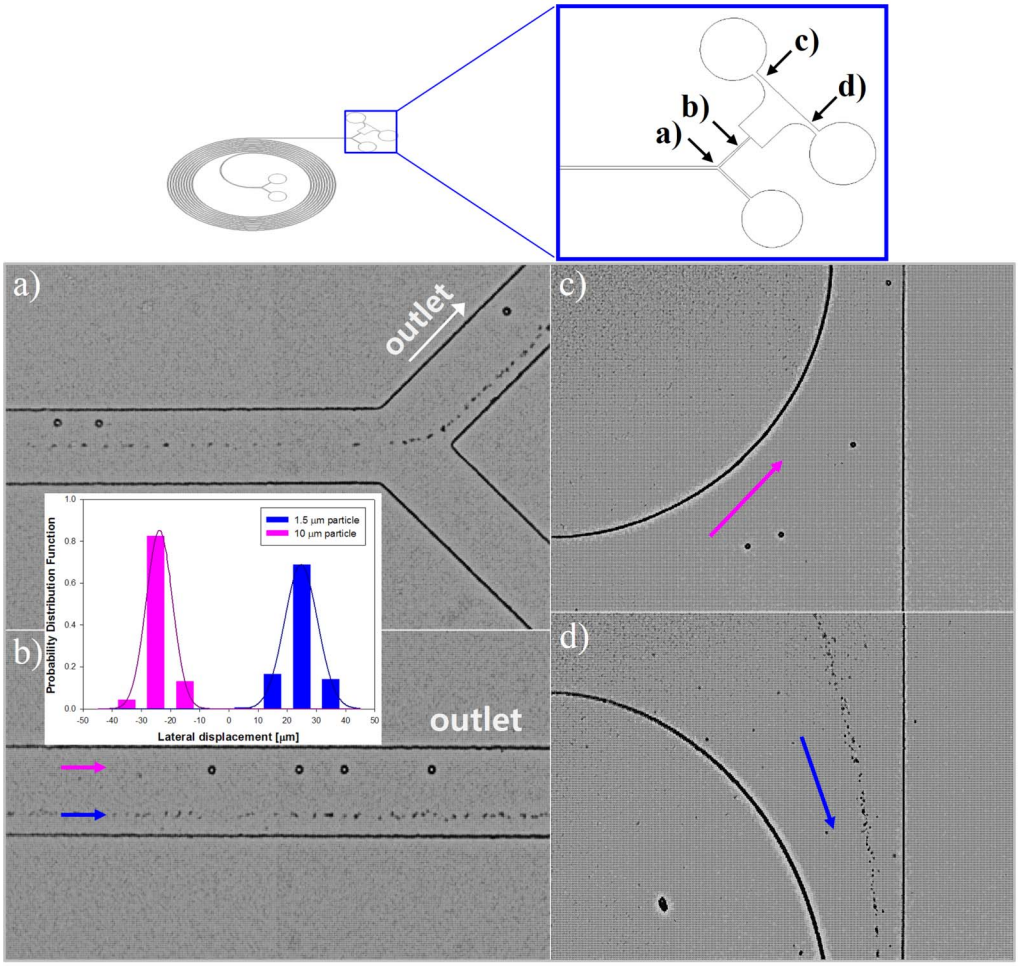

Figure 3 | Experimental results of particle dynamics near an outlet via a viscoelastic medium. (a) and (b) 1.5 and 10 μm PS particles are moved into the upper channel and entrained parallel. (c) and (d) 10 and 1.5 μm PS particles are collected at the upper outlet and the lower outlet, respectively.

and 10 μm PS, respectively. It turns out that the high magnitude of N_1 appears near the inner wall in a spiral channel not like the four-fold symmetry in the straight channel (Fig. 4d and SI movie 3). It shows that $\nabla N_1 / \left|\nabla N_1^{\max}\right|$ is an indicator of the elastic force exerted on the particle because of $F_E \sim a^3 \nabla N_1$, which represents particles can migrate toward the outer wall (Fig. 4e). This asymmetric gradient of N_1 leads the equilibrium position to be off-centered.

Discussion

An elastic force, F_E, can be introduced when a viscoelastic fluid is used as a medium[13,34–36]. The elasticity, inherently present in dilute polymer solutions, can yield particle focusing into the mid-plane of the channel. The particles have different spatial distribution depending on their sizes and rheological properties of the viscoelastic medium. The primary nonlinear elastic force affecting the lateral migration is N_1, since the value of N_1 is normally much greater than N_2[15,18,37]. The relative magnitude of elastic and inertial forces is assessed by the Elasticity number, $El = Wi/Re_c$[38]. N_1 is associated with $Wi = \lambda\dot{\gamma}_c$, which is zero when the fluid is purely viscous, i.e., no elasticity, and increases with increasing the elasticity of fluid. It is worthy to note that Wi is represented as a physical factor to demonstrate the elasticity of the viscoelastic fluid since Wi is determined by the characteristic relaxation time of polymer, a physical quantity of time required for a perturbed polymer chain to return to the equilibrium. Therefore, it is important to characterize Wi to find out an optimal condition for particle focusing from the Wi–De diagram. The use of the elastic force is indeed an appealing method to focus particles at the center of the channel without any external forces and complex geometry. In the literature, small particles with $(a/D_h) < 0.04$ may not successfully be focused due to insufficient length of a straight microchannel[18]. The present spiral channel has approximately 50 cm of arc-length and the length is 10 to 25 times longer than the straight microchannel, which creates the effective elastic force and Dean drag force for the sufficient particle migration regardless of the particle size, e.g., even under $(a/D_h) < 0.04$.

The elastic force generates equilibrium positions at the center and four corners due to N_1 acting on the particle[8,18,38] (Fig. 4a and 4c, and SI movie 1). Particles can be focused at the center as inertial force is increased by increasing the flow rate and F_E becomes large enough (meaning, $Re > 0$ and $Wi > 0$). On the other hand, F_D increases with an increase in Re_c according to the following equations: $De = Re_c \cdot \sqrt{D_h/2R}$ and $F_D \sim func(a,De)$[31]. Since F_D is a function of the particle size and De, the lateral migration behaviors of particles are distinct (Fig. 4b). Here, another Reynolds number is adopted[28] as the particle Reynolds number, $Re_p = Re_c\left(a^2/D_h^2\right) = U_m a^2/\nu D_h$, including parameters for the perturbed channel flow due to suspended particles. We claim that the suspended particles are also perturbed by the secondary flow in a curved spiral channel so that the particle De can also be given by $De_p = Re_p\sqrt{D_h/2R} = Re_c(a/D_h)^2(D_h/2R)^{1/2}$. Hence, the Dean drag force changes significantly with respect to a particle diameter, thereby resulting in a differential lateral migration which is essential for the differential particle focusing. As a consequence, particles have equilibrium positions where the elastic force is determined by De_P.

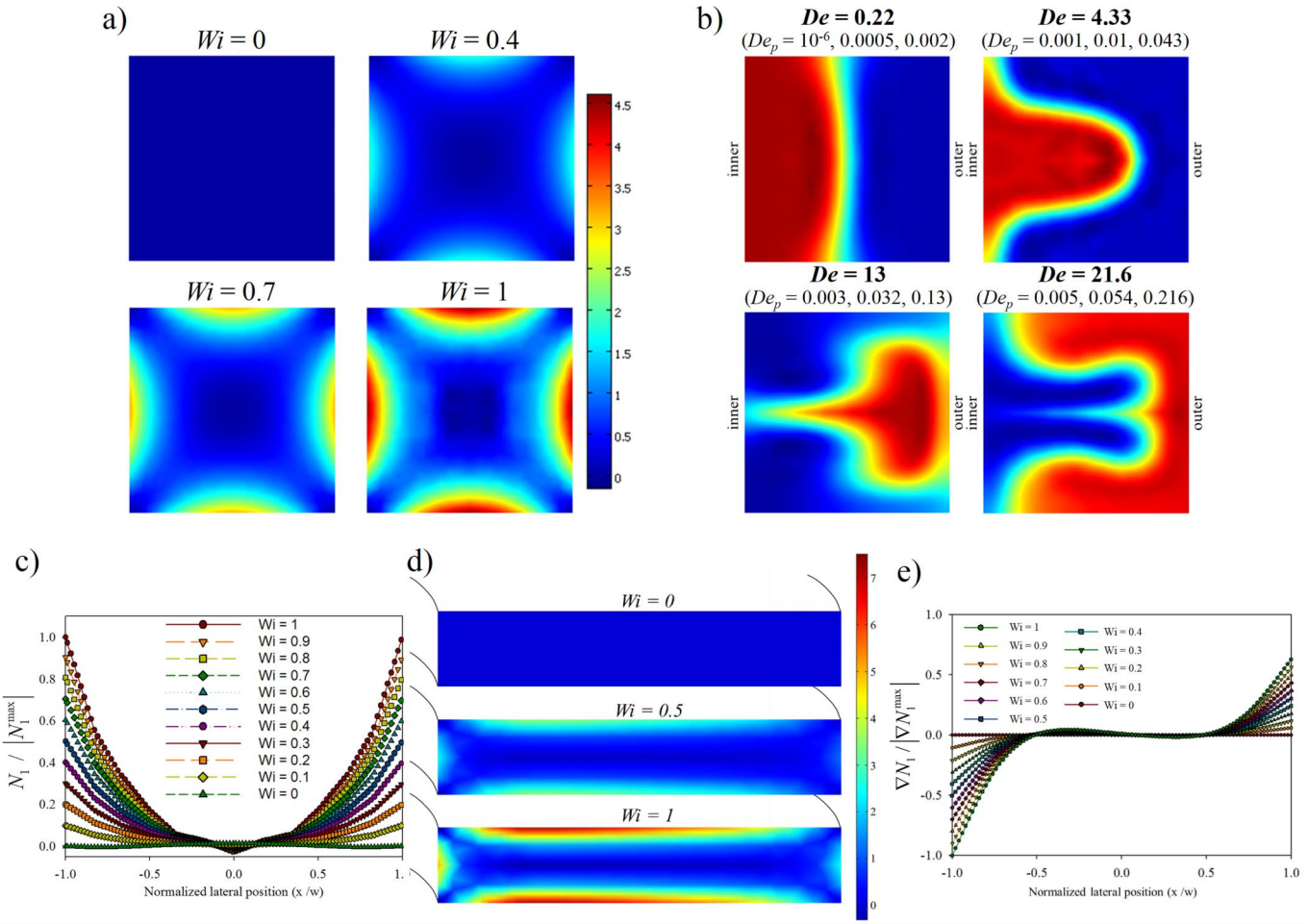

Figure 4 | Numerical simulation of the Dean flow and the first normal stress difference. (a) Results of the first normal stress difference with $Wi = 0$, 0.4, 0.7, and 1 in a straight channel with a channel aspect ratio of 1. The minimum values are found at four corners and the center. (b) Results of the Dean flows for $De = 0.22$, 4.33, 13, and 21.6 in a curved spiral channel with a channel aspect ratio of 1. De_p corresponds to the particle dean number with 1.5, 5, and 10 μm PS, respectively. (c) Normalized first normal stress difference in a straight channel with a channel aspect ratio of 1. It shows nearly zero at $Wi = 0$ and increases with increasing Wi. (d) Results of the first normal stress difference for $Wi = 0$, 0.5, and 1 in a curved spiral channel with a channel aspect ratio of 0.25. It shows an asymmetry, resulting in a lateral migration of particles towards the outer wall. (e) Normalized differential value of the first normal stress difference in a curved channel with a channel aspect ratio of 0.25. The differential value of the first normal stress difference is an indicator of the elastic force exerted on the particle as given by the equation, $F_E \sim a^3 \nabla N_1$.

The main forces related to the present system acting on the suspended particles are F_D and F_E. Here, De_P and $F_D \sim 6\pi\mu a v De_P^2/D_h$ are equated to derive $F_D = 6\eta v \mathrm{Re}_c^2 \delta (a/D_h)^5$, and F_E is expressed as $F_E = Aa^3 \nabla N_1$, which is proportional to the particle size and the differential of N_1. The two forces lead to a scaling law of $(F_D/F_E) \sim a^2 \delta \eta \mathrm{Re}_c^2 / A \nabla N_1 D_h^5$, which helps one to understand physical parameters associated with the equilibrium positions of particles with distinct sizes. F_D and F_E acting on the particles in the microfluidic system were evaluated with use of the calculated quantities, ∇N_1, U_{Dean}, Re_C, and De_P. The relevant results are presented in Fig. 5. F_D significantly increases with decreasing channel height, which implies that the suspended particles tend to move in an outer direction of the channel. The normalized Dean forces significantly increase as the channel aspect ratio (γ) decreases, thereby inducing particle-size dependent lateral migration (Fig. 5a). That is, the particle size is one of the key factors to govern the multiplex particle focusing phenomenon. Conflicting results may be found in two papers: first, Carlo *et al.*[27] demonstrated that F_D decreases with increasing particle size in a given channel aspect ratio since the lateral force and Dean force are complementarily counteracted as $(F_L/F_D) \sim (1/\delta)(a/D_h)^3 R_c^n$. Second, Papautsky *et al.*[31] addressed the dependence of F_L/F_D on the particle size, namely the decrease of F_D with respect to the particle size. Hence, as the ratio increases, the lift force mainly acts on the particles. Since the two researches, however, adopted Newtonian mediums in their experiments, the mid-plane particle focusing band caused by the elastic nature of a viscoelastic medium could not be formed. Therefore, the Dean flow effect on the particle migration could not be developed. In this respect, the proposed multiplex particle focusing offers a noteworthy advantage on differential migration of different size particles as a result of the competition between F_E and F_D. The former is created by the elasticity of the viscoelastic fluid, and the latter is generated in a focusing band region by the geometry of the curved spiral channel.

In addition to the aforementioned, decreasing γ is advantageous for the reduction of Focusing Band Ratio (*FBR*) which is determined by the velocity distribution of Dean flow (SI Fig. 2). Here, *FBR* is defined as (*Focusing Band Height*/*Channel Height*) × 100 [%], which means that the particle-focusing-band-height also decreases with a decrease in *FBR*. The schematic illustration is presented in SI Fig. 2b. The focusing band heights are determined by outward velocity direction in the mid-plane region where particles are focused in the mid-plane (SI Fig. 2a). *FBR* reaches 44% when γ is below 0.5, indicating that the band height is comparable to a particle size of 1.5 μm

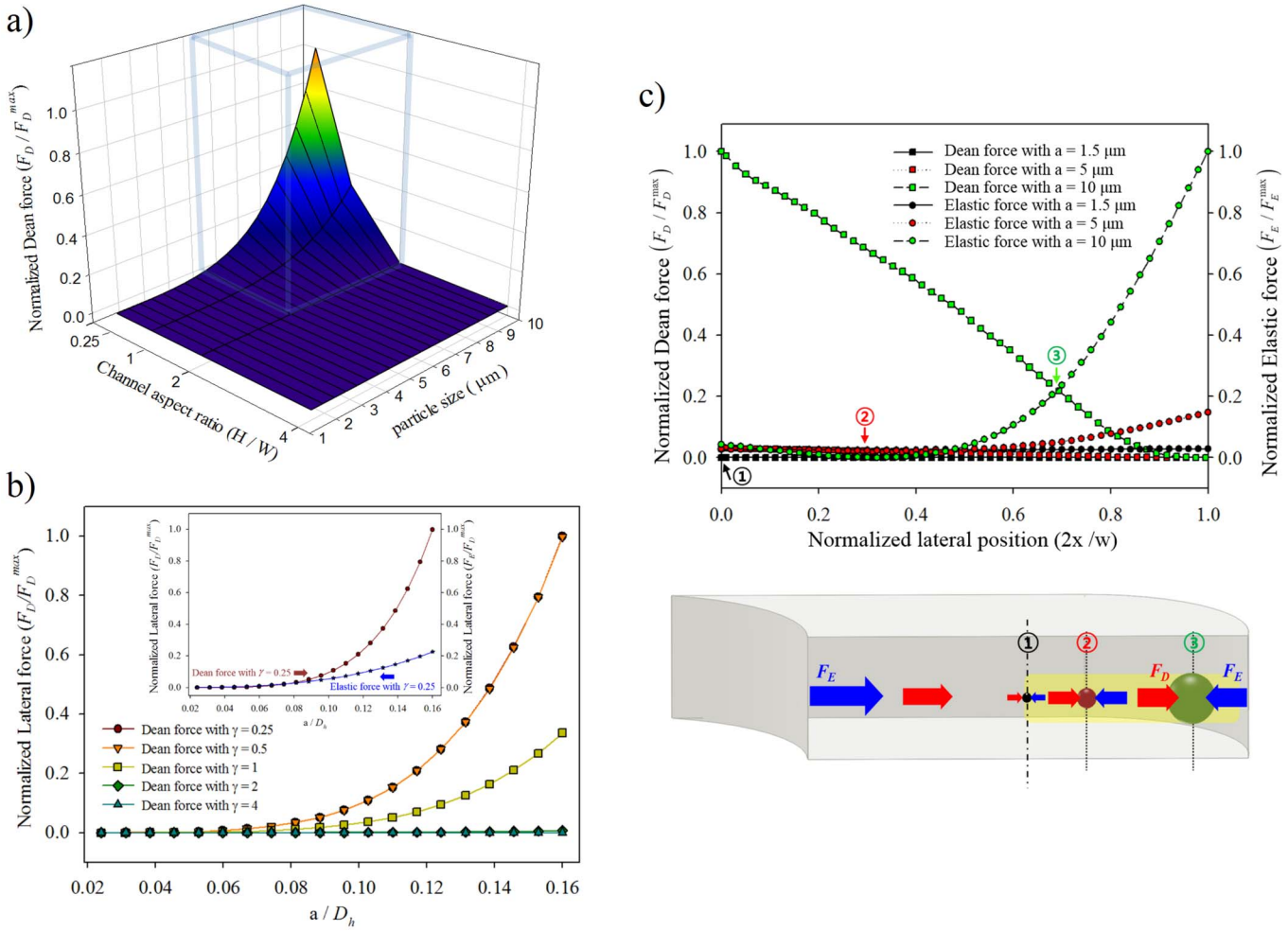

Figure 5 | Numerical results of the Dean drag and elastic forces at the horizontal centerline of the microchannel when $Wi = 1$. (a) Normalized Dean force with respect to channel aspect ratio (H/W) and particle size ranging from 1.5 to 10 μm. A boxed area indicates possible conditions for inducing particle migration. (b) Dean drag forces are normalized with the maximum Dean drag force, indicating the effect of the ratio of particle size to the hydraulic diameter of a microchannel. An inset graph shows both of the dean drag and elastic forces normalized by the maximum Dean drag force under the channel aspect ratio of 0.25. (c) Normalized lateral equilibrium positions of PS particles with 1.5, 5, and 10 μm diameters. A schematic illustration represents net forces acting on the different-sized PS particles.

which results in successful focusing in the mid-plane particle focusing and lateral migration (SI Fig. 2b). The ratio of the particle size to the microchannel dimension, a/D_h, determines whether the system leads to a differential particle migration due to the interaction between F_D and F_E or not. The Dean forces remarkably increase with respect to γ when a/D_h is larger than 0.06 (Fig. 5b), and are almost the same when γ is 0.5 and 0.25. These results reveal that $\gamma = 0.25$ is sufficient to provoke the differential lateral migration by using F_E for the mid-plane focusing and F_D for the lateral migration. Furthermore, the magnitudes of F_D and F_E are significantly different as a/D_h becomes larger than 0.08 in an inset graph; e.g., our system with 100 μm in width and 25 μm in height shows that particle migration is not likely to occur since the magnitudes of F_D and F_E are almost the same causing no difference in net forces acting on the particle. As the particle size is larger than 5 μm, meaning a/D_h is greater than 0.08, F_E becomes more significant than F_D, which leads to the differential particle migration.

The equilibrium positions of particles are determined at which the magnitudes of F_D and F_E are identical. Despite the fact that it is difficult to obtain the exact magnitudes of F_D and F_E quantitatively, the equilibrium positions according to the different particle sizes can be analyzed by using the scaling law. When the particle size is around 1.5 μm, F_E is almost the same as F_D. Therefore, the particles are not laterally migrated, but are focused at the center (Fig. 5c). When the particle size is large enough, e.g., the size is as large as 10 μm, F_D becomes greater than F_E. Thus, the equilibrium position is located at a distance far from the center. This extraordinary particle dynamics according to the particle size is explained with the combination of the elastic force inducing the mid-plane particle focusing and the Dean drag force leading to the particle defocusing from the mid-plane. That is, the combinational manipulation of F_D and F_E is essential to outperform the ability of particle focusing and separation. F_D and F_E play an important role for the separation of different sized particles simultaneously.

The viscoelastic moduli G' and G'' were measured with respect to the angular frequency, which gives the characteristic relaxation time for different kinds of PEO solutions assuming the Maxwell model described by $G'(\omega) = \eta\lambda\omega^2/(1 + \lambda^2\omega^2)$ and $G''(\omega) = \eta\omega/(1 + \lambda^2\omega^2)$, where η is the viscosity, ω is the angular frequency, and λ is the characteristic relaxation time. The characteristic relaxation times for 500, 1000, 3000, and 5000 ppm PEO solutions are estimated to be 0.539×10^3, 1.559×10^3, 3.522×10^3, and 16.1×10^3, respectively. The flow rate was increased from 50 to 750 μl/h to evaluate the value of $Wi = \lambda Q/hw^2$ and plot the Wi–De diagram, where h is the height and w is the width of the curved spiral channel. It is found that multiplex particle focusing initiates when Wi becomes larger than

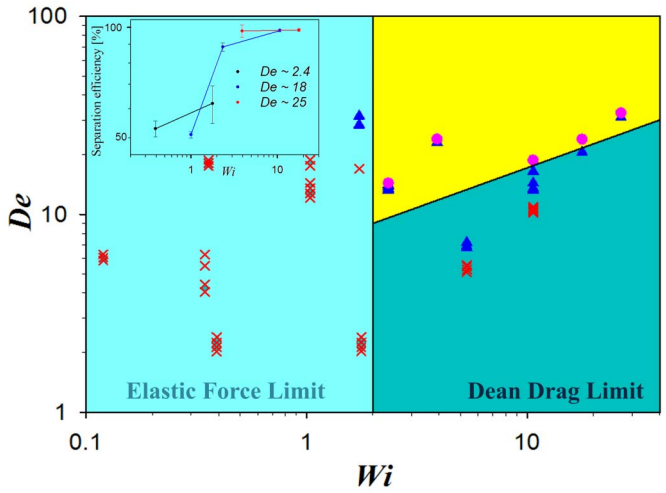

Figure 6 | Experimental results for particle focusing as a function of *De* and *Wi*. No focusing corresponds to red-crosses, single-line focusing blue-triangles, and multiplex focusing pink-circles. An inset graph indicates a separation efficiency with respect to *Wi* and *De*.

2 and *De* is greater than 10 (Fig. 6). The separation efficiency of the proposed system was plotted with respect to *De* (the inset in Fig. 6). The efficiency is very low when $De \sim 2.4$. This is because particles only undergo the elastic force within the channel and are not effectively focused at equilibrium positions depending on their sizes. As the Dean drag force becomes large as much as $De \sim 25$, the efficiency becomes extremely high compared with $De \sim 2.4$ and $De \sim 18$, the efficiency of which is comparable to the highest separation efficiency reported in the literature[31,38–42]. This microfluidic system is capable of acting as a versatile platform that requires only the viscoelastic characteristics of a medium without any additional external forces.

In conclusion, we assert that multiplex particle focusing can be achieved by the fine tuning of the two main forces: the elastic force driven by the nature of a viscoelastic medium and the Dean drag force induced by a curved spiral channel. The particles are situated at an equilibrium position between the two main forces. A numerical simulation was carried out to fully understand the multiplex particle focusing phenomenon. The particle migration towards the outer wall in a focusing band is increased as the particle size becomes larger. Also, it is found that the channel aspect ratio is important to focus particles into the mid-plane of the channel, and that when the focusing band dimension can reach the particle size the particle movement is not perturbed by the Dean vortices but influenced by the lateral Dean drag force and elastic force. It is noticed that particle size-driven multiplex focusing is possible through hydrodynamics encompassing the elastic force and the Dean force. We expect that this study will be able to provide a comprehensive understanding on the particle focusing mechanism which is applicable to various industrial applications ranging from labeling, particle and cell separation, and isolating functionalized particles for biomedical and pharmaceutical practice.

Methods

Experimental methods. Three types of PS particles with 1.5, 5, and 10 μm diameters were used in this study. 1.5, 5, and 10 μm PS particles were purchased from the Bangs Laboratories. A Newtonian fluid was prepared by mixing 22 wt% Glycerin with distilled water to match the densities between the medium and the PS particles. For a viscoelastic fluid, aqueous solutions of polyethylene oxide (PEO, M_w = 1,000,000) with 500, 1000, 3000 and 5000 ppm were used. The Flow rate was increased from 50 to 750 μl/h so as to evaluate various *Wi* and *De*. The PS particles were suspended in both the Newtonian and viscoelastic solutions with a small amount of surfactant (Tween 20, Sigma-Aldrich). The solutions were sonicated for 5 minutes for better dispersion of each particle. Spiral channels with the initial radii of curvatures of 4, 6.6, 8.25, and 9.5 mm were fabricated to evaluate different *De*. All the spiral channels have ten loops, total arc-lengths are approximately 50 cm, and the width and height are set to 100 and 25 μm.

Numerical simulation. We carried out a finite element simulation using the Oldroyd-B model in straight and curved microchannels to solve the viscoelastic behavior of the fluid. For the simulation, governing equations are non-dimensionalized by using Re_c and *Wi*. For steady state, the momentum equation is expressed as $Re(u\cdot\nabla)u = \nabla\cdot(-pI + (\eta_s/\eta)[\nabla u + (\nabla u)^T] + T)$ and the extra stress contribution by the viscoelasticity becomes $T + Wi\,\overset{\nabla}{T} = \left(\eta_p/\eta\right)\left[\nabla u + (\nabla u)^T\right]$, where $\overset{\nabla}{T}$ is the upper convected derivative operator expressed as $\overset{\nabla}{T} = \frac{\partial T}{\partial t} + (u\cdot\nabla)T - \left[(\nabla u)\cdot T + T\cdot(\nabla u)^T\right]$, λ is the characteristic relaxation time, η_s is the relative polymer viscosity, η_s is the relative solvent viscosity, and the total viscosity is $\eta = \eta_s + \eta_p$. The two equations along with the continuity equation are coupled to solve the viscoelastic fluid by varying *Wi* in order to observe the effect of N_1 in the straight and curved microchannels. The relative solvent and polymer viscosities were set to 0.6 and 0.4.

1. Mishra, A., Kavita, K. & Jha, B. Characterization of extracellular polymeric substances produced by micro-algae Dunaliella salina. *Carbohyd Polym* **83**, 852–857 (2011).
2. Lee, K. Y., Peters, M. C., Anderson, K. W. & Mooney, D. J. Controlled growth factor release from synthetic extracellular matrices. *Nature* **408**, 998–1000 (2000).
3. Hu, C. X., Liu, Y. D., Paulsen, B. S., Petersen, D. & Klaveness, B. Extracellular carbohydrate polymers from five desert soil algae with different cohesion in the stabilization of fine sand grain. *Carbohyd Polym* **54**, 33–42 (2003).
4. Davis, B. D. & Tai, P. C. The mechanism of protein secretion across membranes. *Nature* **283**, 433–438 (1980).
5. Milas, M., Rinaudo, M., Knipper, M. & Schuppiser, J. L. Flow and Viscoelastic Properties of Xanthan Gum Solutions. *Macromolecules* **23**, 2506–2511 (1990).
6. Bhat, P. P. *et al.* Formation of beads-on-a-string structures during break-up of viscoelastic filaments. *Nat Phys* **6**, 625–631 (2010).
7. Hur, S. C., Henderson-MacLennan, N. K., McCabe, E. R. B. & Di Carlo, D. Deformability-based cell classification and enrichment using inertial microfluidics. *Lab Chip* **11**, 912–920 (2011).
8. Yang, S. *et al.* Deformability-selective particle entrainment and separation in a rectangular microchannel using medium viscoelasticity. *Soft Matter* **8**, 5011–5019 (2012).
9. Hou, H. W. *et al.* Deformability based cell margination-A simple microfluidic design for malaria-infected erythrocyte separation. *Lab Chip* **10**, 2605–2613 (2010).
10. Janmey, P. A. *et al.* Negative normal stress in semiflexible biopolymer gels. *Nat mater* **6**, 48–51 (2007).
11. Caserta, S., D'Avino, G., Greco, F., Guido, S. & Maffettone, P. L. Migration of a sphere in a viscoelastic fluid under planar shear flow: Experiments and numerical predictions. *Soft Matter* **7**, 1100–1106 (2011).
12. D'Avino, G. *et al.* Single line particle focusing induced by viscoelasticity of the suspending liquid: theory, experiments and simulations to design a micropipe flow-focuser. *Lab Chip* **12**, 1638–1645 (2012).
13. Ho, B. P. & Leal, L. G. Migration of Rigid Spheres in a 2-Dimensional Unidirectional Shear-Flow of a 2nd-Order Fluid. *J Fluid Mech* **7**, 783–799 (1976).
14. Kim, J. Y., Ahn, S. W., Lee, S. S. & Kim, J. M. Lateral migration and focusing of colloidal particles and DNA molecules under viscoelastic flow. *Lab Chip* **12**, 2807–2814 (2012).
15. Leshansky, A. M., Bransky, A., Korin, N. & Dinnar, U. Tunable nonlinear viscoelastic "focusing" in a microfluidic device. *Phys Rev Lett* **98**, 234501 (2007).
16. Romeo, G., D'Avino, G., Greco, F., Netti, P. A. & Maffettone, P. L. Viscoelastic flow-focusing in microchannels: scaling properties of the particle radial distributions. *Lab Chip* **13**, 2802–2807 (2013).
17. Villone, M. M., D'Avino, G., Hulsen, M. A., Greco, F. & Maffettone, P. L. Particle motion in square channel flow of a viscoelastic liquid: Migration vs. secondary flows. *J Non-Newton Fluid* **195**, 1–8 (2013).
18. Yang, S., Kim, J. Y., Lee, S. J., Lee, S. S. & Kim, J. M. Sheathless elasto-inertial particle focusing and continuous separation in a straight rectangular microchannel. *Lab Chip* **11**, 266–273 (2011).
19. Fuh, C. B. & Giddings, J. C. Separation of submicron pharmaceutic emulsions with centrifugal split-flow thin (SPLITT) fractionation. *J Microcol Sep* **9**, 205–211 (1997).
20. Gale, B. K., Caldwell, K. D. & Frazier, A. B. Geometric scaling effects in electrical field flow fractionation. 2. Experimental results. *Anal Chem* **74**, 1024–1030 (2002).
21. Giddings, J. C. Field-Flow Fractionation - Analysis of Macromolecular, Colloidal, and Particulate Materials. *Science* **260**, 1456–1465 (1993).
22. Hwang, W. M., Lee, C. Y., Boo, D. W. & Choi, J. G. Separation of nanoparticles in different sizes and compositions by capillary electrophoresis. *B Kor Chem Soc* **24**, 684–686 (2003).
23. Durr, M., Kentsch, J., Muller, T., Schnelle, T. & Stelzle, M. Microdevices for manipulation and accumulation of micro- and nanoparticles by dielectrophoresis. *Electrophoresis* **24**, 722–731 (2003).

24. Blom, M. T., Chmela, E., Oosterbroek, R. E., Tijssen, R. & van den Berg, A. On-chip hydrodynamic chromatography separation and detection of nanoparticles and biomolecules. *Anal Chem* **75**, 6761–6768 (2003).
25. Giddings, J. C. Eddy Diffusion in Chromatography. *Nature* **184**, 357–358 (1959).
26. Guttman, C. M. & Dimarzio, E. A. Separation by Flow. 2. Application to Gel Permeation Chromatography. *Macromolecules* **3**, 681–691 (1970).
27. Di Carlo, D., Irimia, D., Tompkins, R. G. & Toner, M. Continuous inertial focusing, ordering, and separation of particles in microchannels. *P Natl Acad Sci USA* **104**, 18892–18897 (2007).
28. Di Carlo, D. Inertial microfluidics. *Lab Chip* **9**, 3038–3046 (2009).
29. Yoon, D. H. *et al.* Size-selective separation of micro beads by utilizing secondary flow in a curved rectangular microchannel. *Lab Chip* **9**, 87–90 (2009).
30. Bhagat, A. A. S., Kuntaegowdanahalli, S. S. & Papautsky, I. Continuous particle separation in spiral microchannels using dean flows and differential migration. *Lab Chip* **8**, 1906–1914 (2008).
31. Kuntaegowdanahalli, S. S., Bhagat, A. A. S., Kumar, G. & Papautsky, I. Inertial microfluidics for continuous particle separation in spiral microchannels. *Lab Chip* **9**, 2973–2980 (2009).
32. Bhagat, A. A. S., Kuntaegowdanahalli, S. S., Kaval, N., Seliskar, C. J. & Papautsky, I. Inertial microfluidics for sheath-less high-throughput flow cytometry. *Biomed Microdevices* **12**, 187–195 (2010).
33. Di Carlo, D., Edd, J. F., Humphry, K. J., Stone, H. A. & Toner, M. Particle Segregation and Dynamics in Confined Flows. *Phys Rev Lett* **102**, 094503 (2009).
34. Gan, H. Y., Lam, Y. C. & Nguyen, N. T. Polymer-based device for efficient mixing of viscoelastic fluids. *Appl Phys Lett* **88**, 224103–224103-3 (2006).
35. Groisman, A. & Steinberg, V. Elastic turbulence in a polymer solution flow. *Nature* **405**, 53–55 (2000).
36. Groisman, A. & Steinberg, V. Efficient mixing at low Reynolds numbers using polymer additives. *Nature* **410**, 905–908 (2001).
37. Ho, B. P. & Leal, L. G. Migration of Rigid Spheres in a 2-Dimensional Unidirectional Shear-Flow of a 2nd-Order Fluid. *J Fluid Mech* **76**, 783–799 (1976).
38. Nam, J., Lim, H., Kim, D., Jung, H. & Shin, S. Continuous separation of microparticles in a microfluidic channel via the elasto-inertial effect of non-Newtonian fluid. *Lab Chip* **12**, 1347–1354 (2012).
39. Choi, E., Kim, B. & Park, J. High-throughput microparticle separation using gradient traveling wave dielectrophoresis. *J Micromech Microeng* **19**, 125014 (2009).
40. Lee, M. G., Choi, S. & Park, J. K. Inertial separation in a contraction-expansion array microchannel. *J chromatogr A* **1218**, 4138–4143 (2011).
41. Wu, Z., Willing, B., Bjerketorp, J., Jansson, J. K. & Hjort, K. Soft inertial microfluidics for high throughput separation of bacteria from human blood cells. *Lab Chip* **9**, 1193–1199 (2009).
42. Zhu, J. *et al.* Continuous-flow particle and cell separations in a serpentine microchannel via curvature-induced dielectrophoresis. *Microfluid Nanofluid* **11**, 743–752 (2011).

Acknowledgments

This research was supported by Basic Science Research Program through the National Research Foundation of Korea (NRF) funded by the Ministry of Education, Science and Technology (2013R1A1A2059827). Also, this study was supported by the Korea Science and Engineering Foundation (KOSEF) grant funded by the Korean government (MEST) (R11-2005-065) through the Intelligent Textile System Research Center (ITRC). The authors are grateful for the support.

Author contributions

D.J.L., Y.S.S. and J.R.Y. designed research; Y.S.S. and J.R.Y. supervised the experiments; D.J.L. and Y.S.S. performed research; D.J.L., Y.S.S., H.B. and J.R.Y. analyzed data; D.J.L. wrote the paper. All the authors helped in writing the manuscript, discussed the results and commented on the manuscript.

Additional information

Supplementary information accompanies this paper at http://www.nature.com/scientificreports

Competing financial interests: The authors declare no competing financial interests.

How to cite this article: Lee, D.J., Brenner, H., Youn, J.R. & Song, Y.S. Multiplex Particle Focusing via Hydrodynamic Force in Viscoelastic Fluids. *Sci. Rep.* **3**, 3258; DOI:10.1038/srep03258 (2013).